ACS APPLIED MATERIALS & INTERFACES

Research Article

www.acsami.org

Carbon-Coated Mesoporous TiO_2 Nanocrystals Grown on Graphene for Lithium-Ion Batteries

Zehui Zhang,[†] Ludan Zhang,[‡] Wei Li,*[,‡] Aishui Yu,[‡] and Peiyi Wu*[,†]

[†]State Key Laboratory of Molecular Engineering of Polymers, Collaborative Innovation Center of Polymers and Polymer Composite Materials, Department of Macromolecular Science and Laboratory for Advanced Materials, and [‡]Department of Chemistry, Laboratory of Advanced Materials, Fudan University, Shanghai 200433, China

Supporting Information

ABSTRACT: Graphene-based hybrids have been well studied as advanced catalysts and high-performance electrode materials. In this Article, we have fabricated a novel graphene@mesoporous TiO_2 nanocrystals@carbon nanosheet by a simple one-step solvothermal method. We have found that titanocene dichloride can act as an extraordinary source with multiple roles for forming TiO_2 nanocrystals, ultrathin carbon outer shells, and cross-linkers to binding TiO_2 nanocrystals on graphene surface. Moreover, it also serves as a controlling agent to produce mesoporous structure on TiO_2 nanocrystals. The loading-concentration of mesoporous TiO_2 nanocrystals on graphene sheets can be well controlled by adjusting the initial content of titanocene dichloride. The as-obtained graphene@mTiO_2@carbon nanosheets possess a uniform sandwich-like structure, highly crystalline mesoporous TiO_2 nanocrystals, a high surface area of ~209 m^2/g, and a large pore volume of ~0.68 $cm^3\ g^{-1}$. When used as anodes for LIBs, the resultant nanosheets show a high reversible capacity (~145 mAh/g), good rate capability, and long cycling life (capacity remains 110 mAh/g after 100 cycles at a current density of 0.2 A/g). We believe that our method represents a new path way to synthesize novel nanostructured graphene-based hybrids for future applications.

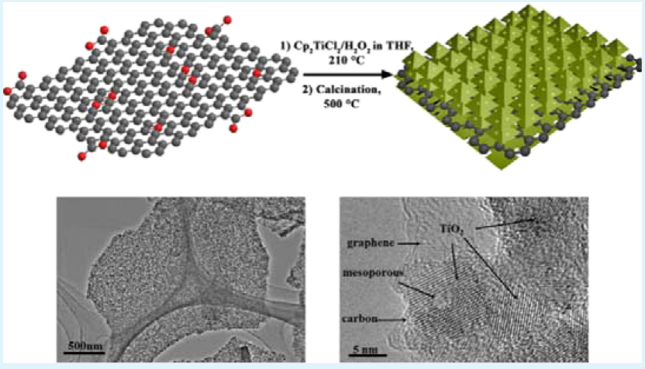

KEYWORDS: *mesoporous, TiO_2 nanocrystals, graphene, carbon, lithium-ion batteries*

1. INTRODUCTION

Graphene, a single layer of honeycomb-like network of carbon atoms, has exceptionally electrical, thermal, mechanical, and optical surface properties and is thought to be one of most promising and striking materials in the 21st century.[1,2] Especially, it has been used as an ideal substrate for fabricating a large number of functional nanohybrids.[3−8] To date, various metal oxides nanoparticles, such as Co_3O_4,[9,10] SnO_2,[11−13] FeO_x,[14−18] TiO_2,[19−26] and MnO_x,[27,28] have been integrated with graphene to overcome their intrinsic shortcomings such as low electrical conductivity, low surface area, and large structural change associated with their applications. As a result, these graphene-based hybrids show improved performances in numerous promising areas including sensor, photocatalysis, solar energy conversion, capacitor, lithium ion batteries (LIBs), and so on.

Several methods have been developed to fabricate graphene-based hybrid materials such as two-step solution process, gas-phase synthesis pathway, and sol−gel method.[29−32] However, a big challenge is the weak interaction between nanoparticles and graphene during the synthetic process, which may hinder the transfer of electrons and Li ions between them, thus impeding applications in catalysis and energy storage.[33,34] Recently, TiO_2 nanomaterials have attracted extensive research interests because of their unique properties and wide applications in catalysis and energy storage.[35−38] It has been found that additives like glucose and polyaniline can be used as the linker and/or face-controlling agent to achieve in situ growth of ultradispersed TiO_2 nanocrystals on the surface of graphene aerogels, but the loading-concentration of TiO_2 nanoparticles is low and cannot be controllable.[39,40] Moreover, during multiple-cycle lithium insertion/extraction processes, TiO_2 nanoparticles would fall off from graphene surface. Recently, a carbon outer shell has been shown to be a valuable protocol to solve the problem; however, it requires additional synthetic processes for coating.[41−46] Therefore, it is still a great challenge and highly desired to accomplish in situ one-pot growth of carbon-coated TiO_2 nanocrystals on graphene with strong binding interactions and controllable loading-concentrations.

Herein, we develop a simple one-step solvothermal method for controllable synthesis of graphene@mesoporous TiO_2 nanocrystals@carbon nanosheets (denoted as graphene@

Received: February 15, 2015
Accepted: April 30, 2015
Published: April 30, 2015

ACS Publications © 2015 American Chemical Society

DOI: 10.1021/acsami.5b01450
ACS Appl. Mater. Interfaces 2015, 7, 10395−10400

Scheme 1. Schematic Illustration for Fabricating Graphene@mTiO$_2$@carbon Nanosheets

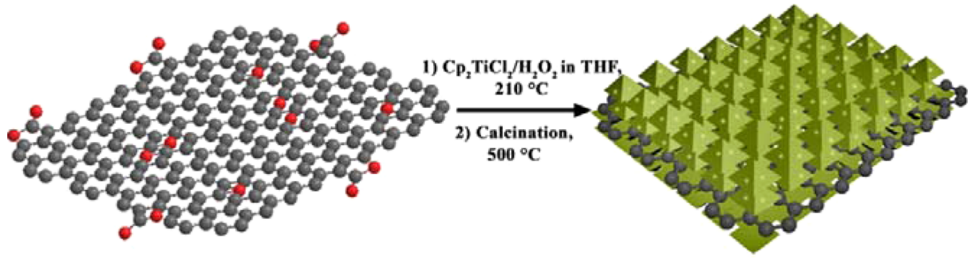

mTiO$_2$@carbon). In this case, GO was first prepared by a modified Hummers method.[47] Titanocene dichloride acts not only as titanium source but also as a carbon precursor for ultrathin carbon outer shells and a cross-linker to binding TiO$_2$ nanocrystals on graphene surface. Moreover, it also serves as a controlling agent to produce mesopores on TiO$_2$ nanocrystals. The loading-concentration of mesoporous TiO$_2$ nanocrystals on graphene sheets can be well controlled by tuning the initial content of titanocene dichloride. The resultant graphene@mTiO$_2$@carbon nanosheets possess a uniform sandwich-like structure, highly crystalline mesoporous TiO$_2$ nanocrystals, a high surface area of ~209 m^2/g, and a large pore volume of ~0.68 cm^3 g^{-1}. When used as anodes for LIBs, the as-obtained nanosheets show a high reversible capacity, good rate capability, and excellent cycling stability.

2. RESULTS AND DISCUSSION

Characterizations of Graphene@mTiO$_2$@carbon Nanosheets. The formation process of the graphene@mTiO$_2$@carbon nanosheets is illustrated in Scheme 1.[18] Detailed experimental steps are described in the Supporting Information. A field emission scanning electron microscopy (FESEM) image of the graphene@mTiO$_2$@carbon nanosheets (Figure 1a, Supporting Information Figure S1) shows that the product is composed of many free-standing and ultrathin sheets with morphology similar to that of initial GO sheets with no naked graphene sheets or free TiO$_2$ nanoparticles, suggesting the uniform TiO$_2$ nanocrystals deposited on graphene sheets. The magnified FESEM images (Figure 1b and Supporting Information Figure S2) clearly disclose a rough surface of the graphene@mTiO$_2$@carbon nanosheets, which results from the loosely packed TiO$_2$ nanocrystals. The magnified FESEM image of nanosheet cross sections (Figure 1c) shows the uniform loading of carbon-coated mesoporous TiO$_2$ nanocrystals on both sides of graphene sheets. TEM images of the nanosheets (Figure 1d) notably show the typical single or overlapping sheetlike morphology but uniformly loading plenty of small nanoparticles, which is consistent with the FESEM results. Figure 1e shows that a large number of TiO$_2$ nanocrystals are densely packed on graphene sheets (Supporting Information Figure S3). The selected area electron diffraction (SAED) pattern (Figure 1e, inset) obviously presents well-resolved diffraction rings, which can be well indexed as the planes of anatase, indicating the existence of TiO$_2$ nanoparticles on graphene sheets.[48] X-ray spectroscopy (EDS) analysis (Supporting Information Figure S4) further confirms the presence of C, Ti, and O elements in the graphene@mTiO$_2$@carbon nanosheets, while the Cu peak originates from the copper grid supporting the sample. HRTEM images (Figure 1f, Supporting Information Figure S5) show that TiO$_2$ nanoparticles are highly crystalline with

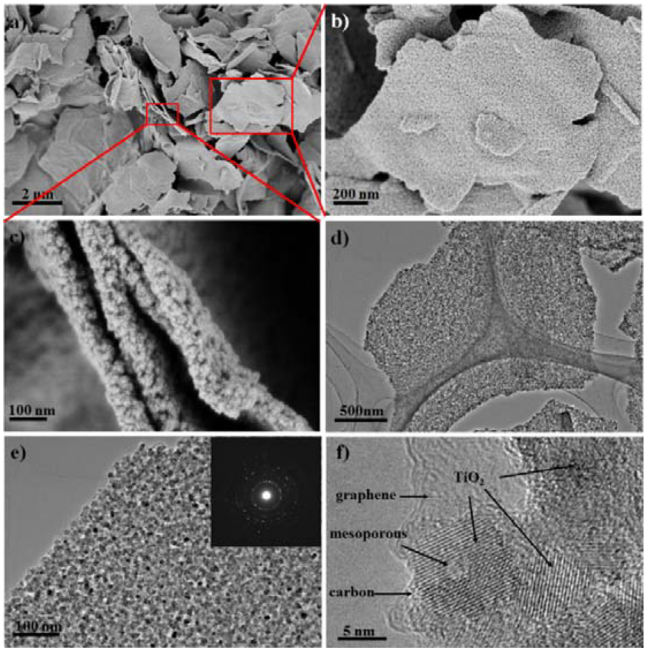

Figure 1. (a–c) FESEM images of graphene@mTiO$_2$@carbon nanosheets. (d, e) TEM images of graphene@mTiO$_2$@carbon nanosheets. Inset in (e) shows the selected electron diffraction pattern of TiO$_2$ nanocrystals on graphene. (f) High-resolution TEM image of graphene@mTiO$_2$@carbon nanosheets.

well-defined crystalline lattices (a *d* spacing of 0.35 nm corresponding to the (101) plane of anatase TiO$_2$) and an average size of ~9 nm on graphene sheets. Additionally, TiO$_2$ nanoparticles are uniformly coated by ultrathin carbon layers. More importantly, one can clearly see mesopores centered in TiO$_2$ nanoparticles (the light-colored part in the center of TiO$_2$).

The uniformly dispersed TiO$_2$ nanoparticles on graphene sheets are further elucidated by the scanning TEM (STEM) image and the corresponding element mapping images (Figure 2) of C, Ti, and O in the graphene@mTiO$_2$@carbon nanosheets. Atomic force microscopy (AFM) analyses (Figure 3) further confirm the 2D features of graphene@mTiO$_2$@carbon nanosheets with a thickness of ~50 nm and a rough surface, which is well consistent with the FESEM and TEM results. As the thickness of the nanosheets is much thicker than the size of TiO$_2$ nanoparticles, we can confirm that TiO$_2$ nanoparticles form a multilayered nanostructure on graphene sheets. XPS spectra confirm that simple pyrolysis of GO sheets in our approach can effectively reduce graphene oxide to graphene (Supporting Information Figure S6).

In the absence of GO sheets, mesoporous TiO$_2$@carbon nanoparticles can be obtained. Transmission electron micros-

DOI: 10.1021/acsami.5b01450
ACS Appl. Mater. Interfaces 2015, 7, 10395–10400

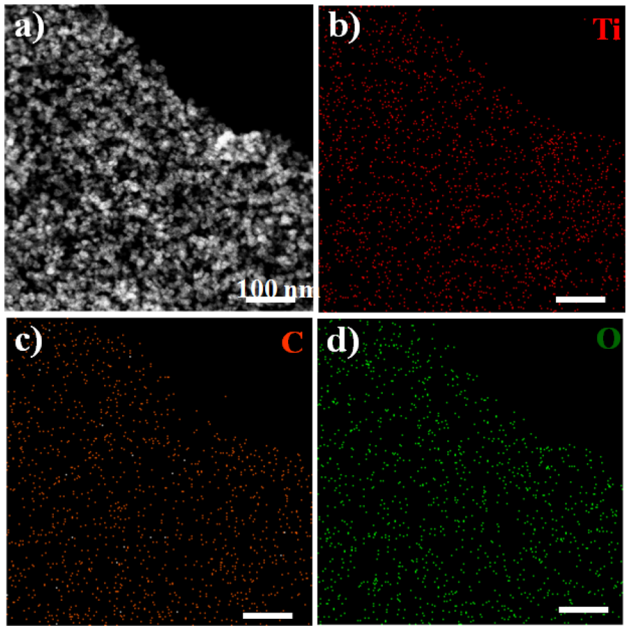

Figure 2. (a) STEM image of the graphene@mTiO$_2$@carbon sheets. (b–d) Corresponding EDX elemental maps of C, Ti, and O, respectively, in (a). It clearly shows that TiO$_2$ nanoparticles are uniformly dispersed on graphene sheets.

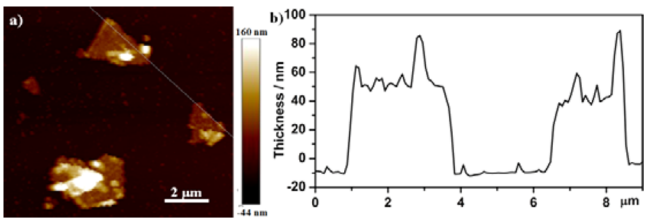

Figure 3. (a) AFM topography images of the graphene@mTiO$_2$@carbon nanosheets on a mica substrate and (b) the corresponding height-profile analysis along the line in (a).

copy (TEM) images notably show that the nanoparticles are core–shell structures with nanoparticle-aggregated TiO$_2$ cores and ultrathin amorphous carbon shells (Supporting Information Figure S7a and S7b), suggesting that the hydrothermal treatment of titanocene dichloride would first trigger the hydrolysis of titanocene into TiO$_2$ cores, followed by the hydrothermal carbonization of cyclopentadienyl into the outer carbon shell. Besides, the cyclopentadienyl can also help form plentiful mesoporous channels in the TiO$_2$ nanocrystals (Supporting Information Figure S7b).

X-ray diffraction (XRD) experiments were carried out to reveal the final composition and structure of graphene@mTiO$_2$@carbon nanosheets. All intense diffraction peaks shown in Figure 4a can be well indexed to anatase TiO$_2$ (JCPDS file no. 21-1272).[21] In addition, no diffraction peaks of the restacking of graphene can be observed, suggesting that the aggregation of graphene sheets during the solvothermal process can be effectively prevented. The weight fractions of TiO$_2$ in the resultant graphene@mTiO$_2$@carbon nanosheets and mTiO$_2$@carbon nanoparticles were detected by thermogravimetric analysis (TGA) (Figure 4b) carried out in air at a heating rate of 10 °C/min. When heated to 800 °C, the carbon component will be completely oxidized to CO$_2$. Based on the final weight ratios after TGA, the content of TiO$_2$ in the resultant graphene@mTiO$_2$@carbon nanosheets and mTiO$_2$@carbon nanoparticles is calculated to be ∼69 and 73 wt %, respectively. Assuming the consistent transformation of titanocene dichloride into TiO$_2$ and carbon, the weight fraction of graphene in the resultant graphene@mTiO$_2$@carbon nanosheets is possibly estimated to be ∼6 wt %.

The pore structures of the resultant graphene@mTiO$_2$@carbon nanosheets and mTiO$_2$@carbon nanoparticles were studied by measuring N$_2$ adsorption/desorption isotherms at 77 K. The BET surface area and pore volume of graphene@mTiO$_2$@carbon nanosheets are calculated to be 209 m^2 g^{-1} and 0.68 cm^3 g^{-1}, higher than that of mTiO$_2$@carbon nanoparticles (181 m^2 g^{-1}, 0.19 cm^3 g^{-1}) (Figure 4c), respectively. The corresponding size distribution curves of graphene@mTiO$_2$@carbon nanosheets and mTiO$_2$@carbon nanoparticles are shown in Figure 4d. The pore size of the nanosheets is mainly 11.3 nm with a wide distribution, which may be originated from the aggregation of TiO$_2$ nanocrystals on graphene and nanosheet itself, respectively. In contrast, mTiO$_2$@carbon nanoparticles have a relatively narrow pore size of ∼7.5 nm.

The influence of the initial titanocene dichloride concentration on the resultant structures of nanosheets was investigated. At a low dosage, aggregated TiO$_2$ nanoparticles are uniformly dispersed on GO sheets (Supporting Information Figure S8a, b). The HRTEM image (Supporting Information Figure S8c) shows that the edge of GO sheets (∼2 layers) can be clearly observed, and the TiO$_2$ nanocrystals (∼9 nm) are mesoporous structure and highly crystalline. Additionally, an ultrathin carbon layer is formed on the surface of TiO$_2$ nanocrystals. With the rise of titanocene dichloride dosage (0.1 g), the density of TiO$_2$ nanoparticles loaded on GO sheets is obviously increased (Supporting Information Figure S8d–f), but the particle size of TiO$_2$ nanocrystals is still ∼9 nm. When the dosage of titanocene dichloride is higher than 0.3 g, graphene@mTiO$_2$@carbon nanosheets would be obtained; however, mTiO$_2$@carbon nanoparticles are concurrently formed and aggregated (Supporting Information Figure S8g, h) due to the excess of titanocene dichloride compared with graphene backbones. These results can also be confirmed by the corresponding FESEM results (Supporting Information Figure S9). Therefore, by rationally controlling the concentration of initial titanocene dichloride, uniform graphene@mTiO$_2$@carbon nanosheets could be obtained, and the density of TiO$_2$ nanoparticles can be facilely tuned.

Electrochemical Performances. The electrochemical performance of graphene@mTiO$_2$@carbon nanosheets and mTiO$_2$@carbon nanoparticles as anode materials for LIBs were evaluated by galvanostatic charge/discharge measurements. Figure 5a shows voltage profiles at the first cycle and the second cyclic performances at a current density of 0.2 A g^{-1} in a voltage window of 1.0–3.0 V, which clearly exhibits two distinct domains. The horizontal discharge plateau is at 1.74 V, and the horizontal charge plateau is at 1.95 V, which are characteristic of intercalation and deintercalation between TiO$_2$ nanoparticles and Li$_{0.5}$TiO$_2$.[49,50] An obvious slope below 1.7 V is also observed which is characteristic of capacitive behavior and results from the improved storage of lithium ions owing to mesoporous structures of TiO$_2$ and the multileveled packed porous structure of nanosheets.[51] As a result, a high capacity of 195 mAh g^{-1} can be delivered in the first discharge with a corresponding charge capacity of 145 mAh g^{-1}. In a control experiment, mTiO$_2$@carbon nanoparticles have a lower capacity of ∼178 mAh g^{-1} in the first discharge with a

DOI: 10.1021/acsami.5b01450
ACS Appl. Mater. Interfaces 2015, 7, 10395–10400

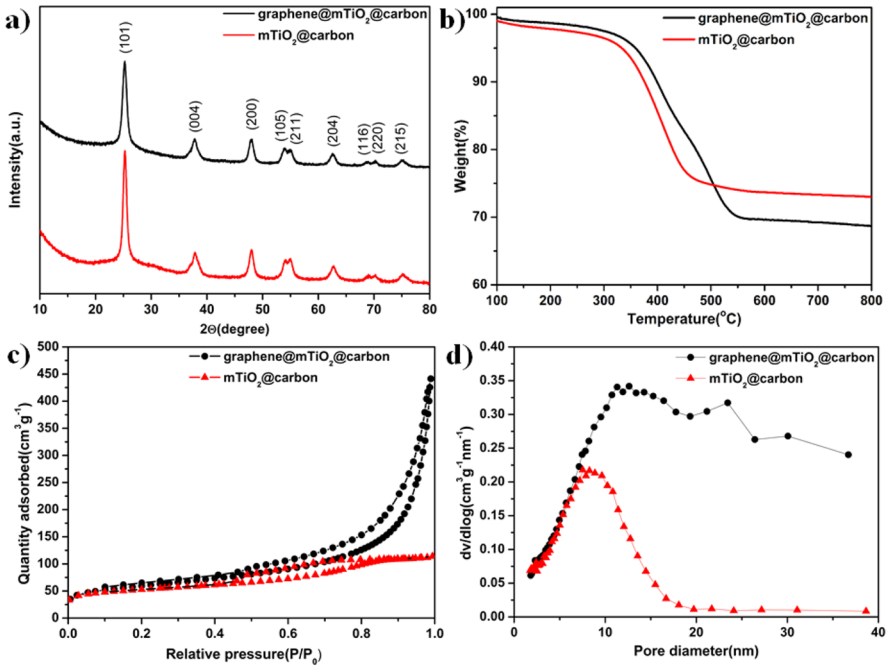

Figure 4. (a) XRD patterns of the graphene@$mTiO_2$@carbon and $mTiO_2$@carbon nanoparticles. (b) TGA curves of graphene@$mTiO_2$@carbon nanosheets and $mTiO_2$@carbon nanoparticles in air. (c) Nitrogen adsorption/desorption isotherms and (d) corresponding pore size distribution curves of graphene@$mTiO_2$@carbon nanosheets and $mTiO_2$@carbon nanoparticles, respectively.

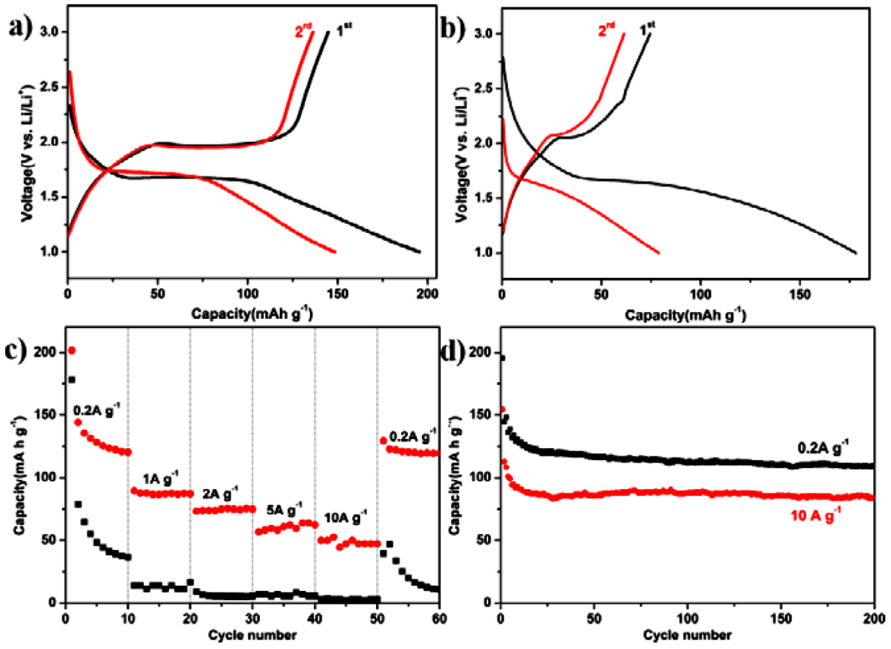

Figure 5. Charge/discharge curves of (a) graphene@$mTiO_2$@carbon nanosheets and (b) $mTiO_2$@carbon nanoparticles at a current density of 0.2 A g^{-1}. (c) Cycling performance of the graphene@$mTiO_2$@carbon nanosheets at constant current densities of 0.2 and 2 A g^{-1}. (d) Cycling performance of the graphene@$mTiO_2$@carbon nanosheets (red) and $mTiO_2$@carbon nanoparticles (black) at different current densities from 0.2 to 10 A g^{-1}. All measurements were conducted within a voltage window of 1.0−3.0 V.

corresponding charge capacity of 76 mAh g^{-1} (Figure 5b). The fast capacity decays of both the graphene@$mTiO_2$@carbon nanosheet and $mTiO_2$@carbon nanoparticle electrodes in the first cycle may be attributed to irreversible reactions with the electrolyte and/or the formation of a solid electrolyte interphase (SEI) layer.[52,53] Figure 5c displays the comparison of cycling performance of the nanosheets at current rates of 0.2 and 2 A g^{-1} in the voltage range of 1.0−3.0 V (vs Li^+/Li) up to 100 cycles. Also, it shows a good cyclic retention of 100 cycles at each current rate and a Coulombic efficiency approaching almost 100% (Supporting Information Figure S10). To investigate the rate capability, the graphene@$mTiO_2$@carbon nanosheets and $mTiO_2$@carbon nanoparticles were discharged and charged at various current rates from 0.2 to 10 A g^{-1} as shown in Figure 5d. Clearly, graphene@$mTiO_2$@carbon nanosheets show better cyclic capacity retention at each

DOI: 10.1021/acsami.5b01450
ACS Appl. Mater. Interfaces 2015, 7, 10395−10400

current density than that of $mTiO_2$@C nanoparticles, which degrade very quickly due to the low content of conductivity agent (carbon black, Super P, 5%). The Nyquist plots show that the charge transfer resistance (R_{ct}) of the graphene@$mTiO_2$@carbon nanosheet electrode is much smaller than that of the $mTiO_2$@carbon nanoparticle electrode (Supporting Information Figure S11). It suggests that the highly conductive graphene and carbon shell could greatly facilitate the charge carrier transfer from TiO_2 nanocrystals to the current collector. It clearly indicates the advantage of such unique nanostructures of nanosheets as anodes for LIBs. Additionally, after the high-current density cyclic, the capacity of graphene@$mTiO_2$@carbon nanosheets at 0.2 A g^{-1} can recover to the initial capacity which indicates its high reversibility. The good electrochemical performances of the graphene@$mTiO_2$@carbon nanosheets may be attributed to synergistic effects in the nanosheets (Supporting Information Figure S12): (1) The ultrathin carbon shell can greatly enhance the internal electrical conductivity and suppress the aggregation of TiO_2 nanocrystals, which thus eventually ensure the stability of the graphene@$mTiO_2$@carbon nanosheet electrode. (2) The small size of primary mesoporous TiO_2 nanocrystal can greatly increase the lithium storage capacity and lithium solid solubility. (3) The graphene nanosheets serve as the conductive medium between the TiO_2 nanocrystals and current collector. As a result, the electrons could be effectively and rapidly conducted back and forth from the TiO_2 nanocrystals to the current collector through the highly conductive graphene nanosheets with the assistant of carbon shell, resulting in good rate capability. (4) The relatively large interface area not only provides more Li^+ insertion/extraction sites but also facilitates fast Li^+ ion transfer between electrode and electrolyte, thus leading to a large reversible specific capacity of the nanosheet electrode.

3. CONCLUSION

In conclusion, we report a one-step solvothermal method for synthesis of graphene@$mTiO_2$@carbon nanosheets. Titanocene dichloride is used as Ti, C source, and the cross-linker to achieve in situ growth of carbon-coated mesoporous TiO_2 nanocrystals on graphene sheets. The as-obtained graphene@$mTiO_2$@carbon nanosheets possess high surface area (~209 m^2/g) and large pore volume (~0.68 cm^3/g). The loading-density of TiO_2 nanoparticles dispersed on graphene sheets can be facilely controlled by adjusting the concentration of titanocene dichloride. The resultant graphene@$mTiO_2$@carbon nanosheets show a high reverse capacity (145 mAh/g), good cycling stability (capacity remains 110 mAh/g after 100 cycles at a current density of 0.2 A/g), and excellent rate performances. This synthetic route describes the blueprint of in situ growth of metal oxide/carbon hybrid materials to extend their functions and achieve specific applications in lithium-ion batteries, sensor, and photocatalysis.

■ ASSOCIATED CONTENT

Supporting Information

Experimental details, FESEM and TEM images; EDX spectra; Coulombic efficiency. The Supporting Information is available free of charge on the ACS Publications website at DOI: 10.1021/acsami.5b01450.

■ AUTHOR INFORMATION

Corresponding Authors

*E-mail: peiyiwu@fudan.edu.cn.

*E-mail: li_w10@fudan.edu.cn.

Notes

The authors declare no competing financial interest.

■ ACKNOWLEDGMENTS

This work was supported by the National Basic Research Program of China (No. 2009CB930000) and NSF of China (No. 20934002, 51073043).

■ REFERENCES

(1) Novoselov, K. S.; Geim, A. K.; Morozov, S. V.; Jiang, D.; Zhang, Y.; Dubonos, S. V.; Grigorieva, I. V.; Firsov, A. A. Electric Field Effect in Atomically Thin Carbon Films. *Science* **2004**, *306*, 666−669.

(2) Geim, A. K.; Novoselov, K. S. The Rise of Graphene. *Nat. Mater.* **2007**, *6*, 183−191.

(3) Stankovich, S.; Dikin, D. A.; Dommett, G. H. B.; Kohlhaas, K. M.; Zimney, E. J.; Stach, E. A.; Piner, R. D.; Nguyen, S. T.; Ruoff, R. S. Graphene-Based Composite Materials. *Nature* **2006**, *442*, 282−286.

(4) Huang, X.; Yin, Z. Y.; Wu, S. X.; Qi, X. Y.; He, Q. Y.; Zhang, Q. C.; Yan, Q. Y.; Boey, F.; Zhang, H. Graphene-Based Materials: Synthesis, Characterization, Properties, and Applications. *Small* **2011**, *7*, 1876−1902.

(5) Li, D.; Kaner, R. B. Materials Science—Graphene-Based Materials. *Science* **2008**, *320*, 1170−1171.

(6) Sun, Y. Q.; Wu, Q. O.; Shi, G. Q. Graphene Based New Energy Materials. *Energy Environ. Sci.* **2011**, *4*, 1113−1132.

(7) Wu, Z. S.; Zhou, G. M.; Yin, L. C.; Ren, W.; Li, F.; Cheng, H. M. Graphene/Metal Oxide Composite Electrode Materials for Energy Storage. *Nano Energy* **2012**, *1*, 107−131.

(8) Huang, C. C.; Li, C.; Shi, G. Q. Graphene Based Catalysts. *Energy Environ. Sci.* **2012**, *5*, 8848−8868.

(9) Wu, Z.-S.; Ren, W.; Wen, L.; Gao, L.; Zhao, J.; Chen, Z.; Zhou, G.; Li, F.; Cheng, H.-M. Graphene Anchored with Co_3O_4 Nanoparticles as Anode of Lithium Ion Batteries with Enhanced Reversible Capacity and Cyclic Performance. *ACS Nano* **2010**, *4*, 3187−3194.

(10) Kim, H.; Seo, D. H.; Kim, S. W.; Kim, J.; Kang, K. Highly Reversible Co_3O_4/Graphene Hybrid Anode for Lithium Rechargeable Batteries. *Carbon* **2011**, *49*, 326−332.

(11) Paek, S. M.; Yoo, E.; Honma, I. Enhanced Cyclic Performance and Lithium Storage Capacity of SnO_2/Graphene Nanoporous Electrodes with Three-Dimensionally Delaminated Flexible Structure. *Nano Lett.* **2009**, *9*, 72−75.

(12) Chen, Y.; Song, B. H.; Chen, R. M.; Lu, L.; Xue, J. M. A Study of The Superior Electrochemical Performance of 3 nm SnO_2 Nanoparticles Supported by Graphene. *J. Mater. Chem. A* **2014**, *2*, 5688−5695.

(13) Zhang, H. W.; Zhou, L.; Yu, C. Z. Highly Crystallized Fe_2O_3 Nanocrystals on Graphene: A Lithium Ion Battery Anode Material with Enhanced Cycling. *RSC Adv.* **2014**, *4*, 495−499.

(14) Chen, Y.; Song, B. H.; Lu, L.; Xue, J. M. Ultra-Small Fe_3O_4 Nanoparticle Decorated Graphene Nanosheets with Superior Cyclic Performance and Rate Capability. *Nanoscale* **2013**, *5*, 6797−6803.

(15) Xia, H.; Hong, C.; Li, B.; Zhao, B.; Lin, Z.; Zheng, M.; Savilov, S. V.; Aldoshin, S. M. Facile Synthesis of Hematite Quantum-Dot/Functionalized Graphene-Sheet Composites as Advanced Anode Materials for Asymmetric Supercapacitors. *Adv. Funct. Mater.* **2015**, *25*, 627−635.

(16) Guo, Y. G.; Hu, Y. S.; Sigle, W.; Maier, J. Superior Electrode Performance of Nanostructured Mesoporous TiO_2 (Anatase) through Efficient Hierarchical Mixed Conducting Networks. *Adv. Mater.* **2007**, *19*, 2087−2091.

(17) Dong, X. M.; Li, L.; Zhao, C. J.; Liu, H. K.; Guo, Z. P. Controllable Synthesis of RGO/Fe_xO_y Nanocomposites as High-Performance Anode Materials for Lithium Ion Batteries. *J. Mater. Chem. A* **2014**, *2*, 9844−9850.

(18) Zhang, Z.; Wang, F.; An, Q.; Li, W.; Wu, P. Synthesis of Graphene@Fe_3O_4@C Core-Shell Nanosheets for High-Performance Lithium Ion Batteries. *J. Mater. Chem. A* **2015**, *3*, 7036−7043.

DOI: 10.1021/acsami.5b01450
ACS Appl. Mater. Interfaces 2015, 7, 10395−10400

(19) Wang, D. H.; Choi, D. W.; Li, J.; Yang, Z. G.; Nie, Z. M.; Kou, R.; Hu, D. H.; Wang, C. M.; Saraf, L. V.; Zhang, J. G.; Aksay, I. A.; Liu, J. Self-Assembled TiO_2-Graphene Hybrid Nanostructures for Enhanced Li-Ion Insertion. *ACS Nano* **2009**, *3*, 907−914.
(20) Cao, X. R.; Tian, G. H.; Chen, Y. J.; Zhou, J.; Zhou, W.; Tian, C. G.; Fu, H. G. Hierarchical Composites of TiO_2 Nanowire Arrays on Reduced Graphene Oxide Nanosheets with Enhanced Photocatalytic Hydrogen Evolution Performance. *J. Mater. Chem. A* **2014**, *2*, 4366−4374.
(21) Li, W.; Wang, F.; Feng, S.; Wang, J.; Sun, Z.; Li, B.; Li, Y.; Yang, J.; Elzatahry, A. A.; Xia, Y.; Zhao, D. Sol−Gel Design Strategy for Ultradispersed TiO_2 Nanoparticles on Graphene for High-Performance Lithium Ion Batteries. *J. Am. Chem. Soc.* **2013**, *135*, 18300−18303.
(22) Li, D.; Shi, D. Q.; Liu, Z. W.; Liu, H. K.; Guo, Z. P. TiO_2 Nanoparticles on Nitrogen-Doped Graphene as Anode Material for Lithium Ion Batteries. *J. Nanopart. Res.* **2013**, *15*, 1674−1676.
(23) Li, W.; Wang, F.; Liu, Y.; Wang, J.; Yang, J.; Zhang, L.; Elzatahry, A. A.; Al-Dahyan, D.; Xia, Y.; Zhao, D. General Strategy to Synthesize Uniform Mesoporous TiO_2/Graphene/Mesoporous TiO_2 Sandwich-Like Nanosheets for Highly Reversible Lithium Storage. *Nano Lett.* **2015**, *15*, 2186−2193.
(24) Mo, R.; Lei, Z.; Sun, K.; Rooney, D. Facile Synthesis of Anatase TiO_2 Quantum-Dot/Graphene Nanosheet Composites with Enhanced Electrochemical Performance for Lithium-Ion Batteries. *Adv. Mater.* **2014**, *26*, 2084−2088.
(25) Qiu, J.; Zhang, P.; Ling, M.; Li, S.; Liu, P.; Zhao, H.; Zhang, S. Photocatalytic Synthesis of TiO_2 and Reduced Graphene Oxide Nanocomposite for Lithium Ion Battery. *ACS Appl. Mater. Interfaces* **2012**, *4*, 3636−3642.
(26) Ren, Y.; Zhang, J.; Liu, Y.; Li, H.; Wei, H.; Li, B.; Wang, X. Synthesis and Superior Anode Performances of TiO_2−Carbon−rGO Composites in Lithium-Ion Batteries. *ACS Appl. Mater. Interfaces* **2012**, *4*, 4776−4780.
(27) You, B.; Li, N.; Zhu, H. Y.; Zhu, X. L.; Yang, J. Graphene Oxide-Dispersed Pristine CNTs Support for MnO_2 Nanorods as High Performance Supercapacitor Electrodes. *ChemSusChem* **2013**, *6*, 474−480.
(28) Duan, J. J.; Chen, S.; Dai, S.; Qiao, S. Z. Shape Control of Mn_3O_4 Nanoparticles on Nitrogen-Doped Graphene for Enhanced Oxygen Reduction Activity. *Adv. Funct. Mater.* **2014**, *24*, 2072−2078.
(29) Huang, X.; Qi, X.; Boey, F.; Zhang, H. Graphene-Based Composites. *Chem. Soc. Rev.* **2012**, *41*, 666−686.
(30) Wang, H. L.; Dai, H. J. Strongly Coupled Inorganic Nanocarbon Hybrid Materials for Energy Storage. *Chem. Soc. Rev.* **2013**, *42*, 3088−3113.
(31) Xiang, Q. J.; Yu, J. G.; Jaroniec, M. Graphene-Based Semiconductor Photocatalysts. *Chem. Soc. Rev.* **2012**, *41*, 782−796.
(32) Guo, S.; Dong, S. Graphene Nanosheet: Synthesis, Molecular Engineering, Thin Film, Hybrids, and Energy and Analytical Applications. *Chem. Soc. Rev.* **2011**, *40*, 2644−2672.
(33) Liang, Y. Y.; Li, Y. G.; Wang, H. L.; Dai, H. J. Strongly Coupled Inorganic/Nanocarbon Hybrid Materials for Advanced Electrocatalysis. *J. Am. Chem. Soc.* **2013**, *135*, 2013−2036.
(34) Etacheri, V.; Yourey, J. E.; Bartlett, B. M. Chemically Bonded TiO_2−Bronze Nanosheet/Reduced Graphene Oxide Hybrid for High-Power Lithium Ion Batteries. *ACS Nano* **2014**, *8*, 1491−1499.
(35) Liu, J.; Zhang, Q.; Yang, J.; Ma, H.; Tade, M. O.; Wang, S.; Liu, J. Facile Synthesis of Carbon-Doped Mesoporous Anatase TiO_2 for the Enhanced Visible-Light Driven Photocatalysis. *Chem. Commun.* **2014**, *50*, 13971−13974.
(36) Xing, M.-Y.; Yang, B.-X.; Yu, H.; Tian, B.-Z.; Bagwasi, S.; Zhang, J.-L.; Gong, X.-Q. Enhanced Photocatalysis by Au Nanoparticle Loading on TiO_2 Single-Crystal (001) and (110) Facets. *J. Phys. Chem. Lett.* **2013**, *4*, 3910−3917.
(37) Xi, Z.; Li, C.; Zhang, L.; Xing, M.; Zhang, J. Synergistic Effect of Cu_2O/TiO_2 Heterostructure Nanoparticle and Its High H_2 Evolution Activity. *Int. J. Hydrogen Energy* **2014**, *39*, 6345−6353.
(38) Li, W.; Wu, Z.; Wang, J.; Elzatahry, A. A.; Zhao, D. A Perspective on Mesoporous TiO_2 Materials. *Chem. Mater.* **2014**, *26*, 287−298.
(39) Qiu, B.; Xing, M.; Zhang, J. Mesoporous TiO_2 Nanocrystals Grown in Situ on Graphene Aerogels for High Photocatalysis and Lithium-Ion Batteries. *J. Am. Chem. Soc.* **2014**, *136*, 5852−5855.
(40) Ma, W.; Han, D.; Gan, S.; Zhang, N.; Liu, S.; Wu, T.; Zhang, Q.; Dong, X.; Niu, L. Rapid and Specific Sensing of Gallic Acid with a Photoelectrochemical Platform Based on Polyaniline−Reduced Graphene Oxide−TiO_2. *Chem. Commun.* **2013**, *49*, 7842−7844.
(41) Su, Y.; Li, S.; Wu, D.; Zhang, F.; Liang, H.; Gao, P.; Cheng, C.; Feng, X. Two-Dimensional Carbon-Coated Graphene/Metal Oxide Hybrids for Enhanced Lithium Storage. *ACS Nano* **2012**, *6*, 8349−8356.
(42) Dong, Y.; Zhao, Z.; Wang, Z.; Liu, Y.; Wang, X.; Qiu, J. Dually Fixed SnO_2 Nanoparticles on Graphene Nanosheets by Polyaniline Coating for Superior Lithium Storage. *ACS Appl. Mater. Interfaces* **2014**, *7*, 2444−2451.
(43) Wang, D.; Yang, J.; Li, X.; Geng, D.; Li, R.; Cai, M.; Sham, T.-K.; Sun, X. Layer by Layer Assembly of Sandwiched Graphene/SnO_2 Nanorod/Carbon Nanostructures with Ultrahigh Lithium Ion Storage Properties. *Energy Environ. Sci.* **2013**, *6*, 2900−2906.
(44) Yue, W.; Tao, S.; Fu, J.; Gao, Z.; Ren, Y. Carbon-Coated Graphene−Cr_2O_3 Composites with Enhanced Electrochemical Performances for Li-Ion Batteries. *Carbon* **2013**, *65*, 97−104.
(45) Jiang, X.; Yang, X.; Zhu, Y.; Yao, Y.; Zhao, P.; Li, C. Graphene/Carbon-Coated Fe_3O_4 Nanoparticle Hybrids for Enhanced Lithium Storage. *J. Mater. Chem. A* **2015**, *3*, 2361−2369.
(46) Zhang, C. F.; Peng, X.; Guo, Z. P.; Cai, C. B.; Chen, Z. X.; Wexler, D.; Li, S.; Liu, H. K. Carbon-Coated SnO_2/Graphene Nanosheets as Highly Reversible Anode Materials for Lithium Ion Batteries. *Carbon* **2012**, *50*, 1897−1903.
(47) Hummers, W. S.; Offeman, R. E. Preparation of Graphitic Oxide. *J. Am. Chem. Soc.* **1958**, *80*, 1339−1339.
(48) Li, W.; Yang, J. P.; Wu, Z. X.; Wang, J. X.; Li, B.; Feng, S. S.; Deng, Y. H.; Zhang, F.; Zhao, D. Y. A Versatile Kinetics-Controlled Coating Method To Construct Uniform Porous TiO_2 Shells for Multifunctional Core-Shell Structures. *J. Am. Chem. Soc.* **2012**, *134*, 11864−11867.
(49) Xin, X.; Zhou, X.; Wu, J.; Yao, X.; Liu, Z. Scalable Synthesis of TiO_2/Graphene Nanostructured Composite with High-Rate Performance for Lithium Ion Batteries. *ACS Nano* **2012**, *6*, 11035−11043.
(50) Chen, J. S.; Liu, H.; Qiao, S. Z.; Lou, X. W. Carbon-Supported Ultra-Thin Anatase TiO_2 Nanosheets for Fast Reversible Lithium Storage. *J. Mater. Chem.* **2011**, *21*, 5687−5692.
(51) Ding, S. J.; Chen, J. S.; Luan, D. Y.; Boey, F. Y. C.; Madhavi, S.; Lou, X. W. Graphene-Supported Anatase TiO_2 Nanosheets for Fast Lithium Storage. *Chem. Commun.* **2011**, *47*, 5780−5782.
(52) Zampardi, G.; Ventosa, E.; La Mantia, F.; Schuhmann, W. In Situ Visualization of Li-Ion Intercalation and Formation of the Solid Electrolyte Interphase on TiO_2 Based Paste Electrodes Using Scanning Electrochemical Microscopy. *Chem. Commun.* **2013**, *49*, 9347−9349.
(53) Methekar, R. N.; Northrop, P. W. C.; Chen, K. J.; Braatz, R. D.; Subramanian, V. R. Kinetic Monte Carlo Simulation of Surface Heterogeneity in Graphite Anodes for Lithium-Ion Batteries: Passive Layer Formation. *J. Electrochem. Soc.* **2011**, *158*, A363−A370.

DOI: 10.1021/acsami.5b01450
ACS Appl. Mater. Interfaces 2015, 7, 10395−10400